

RSC Advances



This is an *Accepted Manuscript*, which has been through the Royal Society of Chemistry peer review process and has been accepted for publication.

Accepted Manuscripts are published online shortly after acceptance, before technical editing, formatting and proof reading. Using this free service, authors can make their results available to the community, in citable form, before we publish the edited article. This *Accepted Manuscript* will be replaced by the edited, formatted and paginated article as soon as this is available.

You can find more information about *Accepted Manuscripts* in the [Information for Authors](#).

Please note that technical editing may introduce minor changes to the text and/or graphics, which may alter content. The journal's standard [Terms & Conditions](#) and the [Ethical guidelines](#) still apply. In no event shall the Royal Society of Chemistry be held responsible for any errors or omissions in this *Accepted Manuscript* or any consequences arising from the use of any information it contains.

1 Fabrication of superhydrophobic thin films on
2 various substrates using SiO₂ nanoparticles coated
3 with polydimethylsiloxane: towards development of
4 shielding layers for gas sensors

5 *Eun Ji Park¹, Bo Ra Kim¹, Dae Keun Park, Sang Wook Han, Dae Han Kim,*

6 *Wan Soo Yun and Young Dok Kim**

7 Department of Chemistry, Sungkyunkwan University, 440-746 Suwon, Republic of Korea

8 E-mail: ydkim91@skku.edu

9 **Abstract**

10 Superhydrophobic membranes with high gas permeability were prepared and characterized.
11 Materials such as metal mesh, paper, fabric, and polytetrafluoroethylene were dip-coated in a
12 hexane-based solution of SiO₂ nanoparticles coated with polydimethylsiloxane (PDMS). The
13 dip-coating provided a superhydrophobic characteristic to the surfaces of our membranes with
14 water contact angles exceeding 160°. On the other hand, high membrane permeability of CO₂
15 and dimethyl methylphosphonate vapor were obtained, indicating that our preparation method is
16 useful for the fabrication of gas sensor shielding layers that allow selective permeation of gas
17 vapor from gas/aqueous-liquids mixtures.

1 Introduction

2 Superhydrophobicity refers to the surface property of a water contact angle exceeding $\sim 150^\circ$,
3 which can result from a combination of dual surface roughness and hydrophobic surface
4 functionality.¹⁻⁴ A hierarchical surface structure forming dual surface roughness can minimize
5 the contact area between the solid surface and a water droplet, resulting in water repellent
6 properties.

7 A superhydrophobic surface can be prepared by patterning a flat solid and hydrophobic
8 surface, resulting in a hierarchal surface structure.^{5,6} Alternatively, distribution of hydrophobic
9 nanoparticles can result in a superhydrophobic surface, since nanoscale surface roughness due to
10 the intrinsic particle size superposes the (sub) micrometer-scale roughness formed by the
11 agglomeration of nanoparticles.⁷⁻⁹ Diverse strategies for a more facile and economic fabrication
12 of superhydrophobic surfaces have been developed, and the improved chemical and mechanical
13 stability of superhydrophobic surfaces have received broad interest.¹⁰⁻¹⁶

14 Superhydrophobicity is of great interest in various fields. Superhydrophobic foams can be used
15 for selectively isolating oil from oil/water mixtures, and this technology is related to efficient
16 removal of spilled oil from global waters.¹⁷⁻¹⁹ Superhydrophobic surfaces can also show self-
17 cleaning behaviors, i.e., dust particles existing on superhydrophobic surfaces can be swept away
18 from the surface by rolling water droplets.²⁰⁻²³ When such self-cleaning properties can be
19 combined with high optical transparency of thin films, many interesting applications become
20 possible, such as in photovoltaic panels.²⁴⁻²⁶

21 Many chemical sensors, playing a crucial role in environmental science and technology, are
22 based on the detection of vapors, and these sensors are often easily contaminated by the
23 introduction of aqueous liquids.²⁷⁻²⁹ A shielding layer in the aperture of the sensor can be used to

1 protect the sensor from aqueous liquids and allow selective permeation of gas molecules, which
2 can ultimately protect the vapor sensor from the fatal contamination by aqueous liquid. In the
3 present study, we developed a wet-chemical process for the preparation of such shield layers,
4 thereby inhibiting permeation of aqueous liquids and allowing gas transmission. Our method is
5 based on simple and cost-effective wet-chemical dip coating and SiO₂ nanoparticles coated by
6 polydimethylsiloxane (PDMS).³⁰⁻³⁵

8 Experiments

10 Materials

11 Silica nanoparticles (Degussa, Aerosil 200, mean particle size = 24 nm), hexane (DAEJUNG,
12 purity = 100%), ethanol (DAEJUNG, purity = 95%) and fluidic PDMS (Dow Corning, Sylgard
13 184) were used as received. The average molecular weight (M_n), weight average molecular
14 weight (M_w) and polydispersity index (PDI) of PDMS used in this work were ~4200 g/mol,
15 ~14000 g/mol and 3.3, respectively (measured by gel permeation chromatography; GPC, Agilent
16 1100s). Two types of polytetrafluoroethylene (PTFE) membranes were purchased from Meari,
17 one with pore size of 0.2 μm and membrane thickness of 30 μm (PTFE-1) and the other one 5,
18 and 100 μm of the respective values (PTFE-2). Stainless steel-meshes with different pore sizes
19 (100 mesh and 165 mesh) were obtained from Ehwa Chulmang, and are denoted as Mesh-1
20 (rectangular pores with a side length of 141 μm and a wire diameter of 100 μm) and Mesh-2
21 (rectangular pores with a side length of 100 μm, and a wire diameter of 53 μm), respectively.
22 Paper (80 m²/g), cotton fabrics (Fabric-1: 30 counts, Fabric-2: 100 count) and umbrella fabric
23 were obtained from a local store.

1 **Preparation of hydrophobic silica nanoparticles**

2 In order to fabricate PDMS-coated silica nanoparticles, a thermal vapor deposition method was
3 used. Bare silica nanoparticles and fluidic PDMS were combined at a weight ratio of 1:1 in a
4 stainless steel reactor. PDMS and bare silica nanoparticles were separated with a metal mesh (30
5 mesh) partition (Fig. 1a). Then, the reactor was sealed with polyimide (PI) tape and heated to
6 300 °C for 15 h. The reactor was equipped with a power supply, k-type thermocouple, heating
7 band, and temperature controller. Using this procedure, PDMS vapor was deposited on the
8 surfaces of bare silica nanoparticles, forming a thin PDMS layer.

10 **Dip coating**

11 Solution A was prepared by dispersing PDMS-coated silica nanoparticles (0.2 g) in hexane (29
12 ml), and solution B was a mixture of solution A (29 ml) and an adhesive solution (1 ml), which
13 was prepared by dissolving PDMS (1 ml) and curing agent (0.1 ml) in hexane (8 ml).

14 Metal mesh-1 was used as a substrate for dip coating. The mesh surface was cleaned in ethanol
15 for 10 min, wiped clean, and dried at room temperature. The mesh was dipped into Solution B
16 for 10 sec, placed vertically, and dried for 5 min under atmospheric conditions. This dip coating
17 process was repeated three times. Hereafter, the mesh-1 coated with solutions B and A are
18 referred to as mesh-1B and mesh-1A, respectively. Other substrates, mesh-2, PTFE-1 and 2,
19 fabric-1 and 2 and paper, were coated using the same method (Fig. 1b).

21 **Characterizations**

22 For the characterization of the chemical structure of bare and PDMS-coated nanoparticles, X-
23 ray photoelectron spectroscopy (XPS) and Fourier transform infrared (FT-IR, BRUKER,

1 Optics/vertex 70) spectroscopy were used. The XPS system was equipped with concentric
2 hemispherical analyzer (CHA, SPECS, PHOIBOS-Has 3500) and Mg K α -source (1253.6 eV).
3 XPS spectra were obtained under a base pressure of 2.0×10^{-9} torr. Static and dynamic water
4 contact angles were measured for characterizing the surfaces consisting of PDMS-coated silica
5 nanoparticles using a Theta optical tensiometer (KSV Instruments, Ltd.) equipped with a digital
6 camera connected to a computer; Young–Laplace curves were employed for the fitting process
7 required for contact angle determination. The static contact angle was measured by dropping ~ 5
8 μ l of distilled water onto the surface, and the dynamic contact angle while gradually adding and
9 removing water from the water droplet. Contact angle hysteresis was determined by the
10 difference between advancing and receding contact angles. The advancing contact angle is the
11 maximum contact angle obtained upon adding water volume, while the receding contact angle is
12 the minimum contact angle observed during receding water volume. Contact angle values were
13 the averages of three measurements at different spots on each sample. In order to analyze
14 structures and chemical elements of surfaces before and after dip-coating on substrates, scanning
15 electron microscopy (SEM, JEOL, JEM-2100F) equipped with energy dispersive spectrometry
16 (EDS) and atomic force microscopy (AFM, Park system, NX-10) were used. In order to
17 determine the chemical stability of mesh-B, the sample was exposed to acidic (HCl (aq), pH 2.5)
18 and basic (NaOH (aq), pH 12) solutions for 40 min or UV irradiation (VILBER LOUGMAT,
19 UV lamp, $\lambda = 254$ nm) for 80 h.

20

21 **Sand abrasion test**

22 To evaluate the mechanical resistance of fabricated dip-coating films with and without
23 adhesives, a sand abrasion test was conducted in the following conditions: sand (20 g in each

1 test) was dropped from a 30 cm height onto fabricated films, at a tilt angle of 45° with respect to
2 the axis vertical to the bottom surface of the experimental set-up (Fig. 2a). Average particle size
3 of the sand was 100 μm and its velocity at impact was about 0.22 ms^{-1} in our experimental
4 conditions.

6 **Gas permeation test**

7 In order to evaluate the gas permeability of the fabricated films using solution B, a gas
8 permeation test was performed using a CaCO_3 precipitation reaction (Fig. 2b). A $\text{Ca}(\text{OH})_2$
9 aqueous solution (20 mL, 4 mM) was added to three vials, and printed letters were attached to
10 the sidewall of the vials such that the letters could be seen. A hazy aqueous solution, which
11 indicated the presence of a precipitate, was formed by diffusion of CO_2 gas into the glass reactor.
12 After sealing the glass reactor, CO_2 gas was continuously flowed through the reactor at 30
13 pounds per square inch (psi). Information regarding gas permeability of the fabricated films was
14 qualitatively obtained based on letter clarity.

15 Gas permeability was quantitatively determined using solid phase micro-extraction (SPME)
16 and gas chromatography (GC). An SPME fiber (divinylbenzene (DVB)/carboxen (CAR)/PDMS
17 fiber, SUPELCO, 50/30 μm thickness) was placed in a vial containing a smaller vial filled with
18 dimethyl methylphosphonate (DMMP, Sigma-Aldrich, 97%) (Fig. 2c). The smaller vial was
19 either open or sealed with films having a superhydrophobic coating, and the DMMP vapor was
20 extracted through the SPME fiber above the smaller vial for two minutes. During the extraction
21 process, the vial and fiber temperature was kept at 50 °C. The extracted DMMP on the SPME
22 fiber surface was subsequently desorbed and analyzed using gas chromatography (GC, HP 6890,
23 Agilent Technologies).

1 **Static column water resistance test**

2 Static column water resistance test was performed based on ISO-811 standard method to
3 evaluate waterproof ability of the fabricated samples. The bottom part of a column was sealed
4 with the fabricated films and distilled water was poured from the top. The water level at which
5 the water begins to penetrate the film was recorded and the test was performed three times for
6 each sample.

8 **Result and discussion**

10 **Characterizations of bare and PDMS-coated silica nanoparticles**

11 The surface chemical compositions of bare and PDMS-coated silica nanoparticlea were
12 analyzed using XPS (Fig. S1). In the Si 2p core-level spectra, the bare sample showed a peak
13 centered at 103 eV, and additional PDMS-coating resulted in appearance of a shoulder at ~101
14 eV. The intensity of the C 1s peak centered at 284.1 eV was increased upon PDMS-coating due
15 to the methyl group in the framework of PDMS.³⁶ The intensity ratio of Si 2p and C 1s peaks
16 attributed to the PDMS layer was 2.19, which is similar to the atomic ratio of Si and C in the
17 PDMS framework. Surface functional group of bare and PDMS-coated silica nanoparticles was
18 investigated with FT-IR (Fig. 3a). Before PDMS-coating on silica nanoparticles, a Si-O-Si
19 asymmetric stretching band centered at 1095 cm^{-1} and a Si-O-Si symmetric stretching band
20 located at 810 cm^{-1} were observed in the FT-IR spectra.^{37, 38} After the PDMS-coating of bare
21 silica nanoparticles, additional vibrational features of PDMS included an sp^3 C-H stretching
22 mode^{39, 40} located at 3000 cm^{-1} and 2900 cm^{-1} and the CH_3 deformation of Si- CH_3 observed at
23 ~1400 cm^{-1} .⁴¹ Note that, in the previous study, it was confirmed that peaks of PDMS-coated

1 silica nanoparticles prepared using the same method corresponded to those of PDMS elastomer
2 in terms of band position, which means that PDMS-layer deposited on silica nanoparticles has no
3 significant structural change with regard to the pristine PDMS.³³ Considering the FT-IR and XPS
4 results, one can expect that the dimethylsiloxane network of PDMS was preserved after the
5 deposition on silica nanoparticles. In order to confirm the water-repellent properties of silica
6 nanoparticles after PDMS coating, 0.2 g of either bare or PDMS-coated silica nanoparticles were
7 placed in vials filled with 20 ml of distilled water. Fig. 3b shows that bare silica nanoparticles
8 were almost completely mixed with distilled water, whereas PDMS-coated silica nanoparticles
9 floated on the water.

10

11 **Surface characterizations before and after dip-coating on substrates**

12 The static water contact angle values (θ_{sta}) of samples before and after dip-coating in solution
13 B and water contact angle hysteresis ($\theta_{\text{ad}} - \theta_{\text{re}}$) of the substrates after dip-coating were measured
14 for various substrates, as shown in Table 1. The θ_{sta} values of uncoated substrates were smaller
15 than 150° , whereas those of the coated-substrates were larger than 150° . In addition, for dip-
16 coated substrates, the water contact angle hysteresis values were determined to be less than 10°
17 (Table 1). All substrates used in this work became superhydrophobic after dip-coating. It is
18 worth mentioning that the use of the solutions A instead of B for the dip-coating resulted in
19 almost the same water contact angles (result of the solution A not shown here).

20 The significant change in surface structure before and after dip-coating the metal mesh-1 with
21 the solution B was confirmed with SEM images (Fig. 4). As shown in Fig. 4b, the wire of the
22 plain metal mesh-1 was originally smooth and, after dip-coating (mesh-1B), the wires were
23 randomly covered with PDMS-coated silica nanoparticles, which resulted in an increased

1 roughness of the wire surface (Fig. 4c). High magnification (Fig. 4d) clearly shows that
2 aggregation of hydrophobic-coated silica nanoparticles produced surface roughness on the
3 micrometer scale. The EDS element mapping images (Figs. 4e and f) show that the particles
4 adhered to the mesh-1B surface consisted of Si and C, each originating from silica nanoparticles,
5 and a PDMS thin layer present on the silica and adhesives, respectively. Since micrometer-scale
6 roughness caused by aggregations of PDMS-coated silica nanoparticles superposes the
7 nanoscale-roughness induced by the intrinsic sizes of individual nanoparticles, superhydrophobic
8 surface properties are produced. Here again, the use of the solutions A and B resulted in almost
9 the same surface morphology characterized by the SEM (SEM images of the mesh-1A are not
10 shown here).

11

12 **Surface stability after dip-coating on a substrate**

13 In order to examine the effect of PDMS adhesive on the superhydrophobic stability, a sand
14 abrasion test was performed for mesh-1A and mesh-1B. Fig. 5 shows the change in water contact
15 angle as a function of the amount of sand dropped onto the surface. Prior to the test, all the
16 samples showed superhydrophobic properties with water contact angles exceeding 160° . With an
17 increasing amount of sand dropped onto the sample surface, the water contact angle gradually
18 decreased due to mechanical abrasion. However, when the total amount of fallen sand exceeded
19 60 g, the contact angles of mesh-1A and mesh-1B showed a significant difference; after 100 g,
20 only mesh-1B maintained a superhydrophobic property with a water contact angle of $\sim 150^\circ$.
21 However, mesh-1A showed a much lower water contact angle ($\sim 120^\circ$). This result implies that
22 the superhydrophobic surface of mesh-1B was mechanically more stable than that of mesh-1A.
23 Comparing the SEM images in Fig. 6 after the sand abrasion test with those of Figs. 4c and d

1 before the test, many SiO₂ nanoparticles on mesh-1A were removed during the sand abrasion test
2 (Fig. 6b), whereas mesh-1B showed few changes in the surface structure after the sand abrasion
3 test (Fig. 6d). This result suggests that PDMS-coated silica nanoparticles attached to mesh-1B
4 were more stable than those bound to mesh-1A due to the existence of adhesives in the dip-
5 coating solution B.

6 In order to shed light on more details of the the surface morphology of mesh-1A and mesh-1B,
7 AFM analyses were carried out (Fig. S2). It is clearly shown that, by dip-coating with either
8 solution A or B, the nanometer-scale roughness has been increased by PDMS-coated silica
9 nanoparticles covering the surface. For mesh-1A, rough feature of the surface disappeared after
10 the sand test whereas it was maintained to some extent on mesh-1B, i.e., PDMS-coated silica
11 nanoparticles on the surface was washed away on mesh-1A but remained intact on mesh-1B
12 upon sand abrasion. A similar result can also be seen for PTFE substrates, even though the
13 change in the surface morphology of paper upon dip-coating could be hardly seen, due to the
14 intrinsically high roughness of the paper surface (Fig. S3). For fabric, the surface roughness was
15 so high that AFM measurement could be hardly performed. It is worth mentioning that root mean
16 square (rms) roughness values summarized in Fig. S4 should be taken with care since the value
17 includes the intrinsic roughness of substrates, which is quite high, and also vary much depending
18 on the local positions of the surface. More importantly, alteration in the sub-micrometer and
19 nanometer scale structures upon coating should be more carefully considered.

20 After being exposed to two different pH conditions and UV irradiation, the chemical stability
21 of mesh-1B was evaluated by measuring the water contact angle after each treatment. The
22 sample was immersed into either acidic (HCl (aq), pH 2.5) or basic (NaOH (aq), pH 12) solution
23 for 40 min, washed with distilled water, and dried before measuring the water contact angle. As

1 shown in Fig. 7a, the water contact angle did not change significantly after the acid/base
2 treatment, i.e., the superhydrophobicity of the mesh-1B surface was sustained under harsh
3 chemical conditions. In addition, when the surface of mesh-1B was irradiated by UV light (245
4 nm, 4 W) for 80 h, the surface maintained its water contact angle greater than 160° (Fig. 7b).

6 **Gas permeability and waterproof ability of fabricated films**

8 The gas permeability of mesh-1B was tested with a simple experimental design, shown in Fig.
9 2b: a vial without a cap (open, ①), a vial wrapped with fabricated film (②), and a vial sealed
10 with a cap (③) were placed in a glass bottle with a branch for CO_2 gas injection. In each vial was
11 20 ml of $\text{Ca}(\text{OH})_2$ aqueous solution, which produces a precipitate, $\text{Ca}(\text{CO}_3)_2$, by reacting with
12 CO_2 gas. Fig. 8 shows images of the vials before and after CO_2 gas injection. Before the
13 injection, the $\text{Ca}(\text{OH})_2$ aqueous solutions in each vial were clear, whereas the solutions in vials
14 ① and ② became turbid after injecting CO_2 gas at 30 psi, indicating that CO_2 gas molecules had
15 permeated through the fabricated film and reacted with $\text{Ca}(\text{OH})_2$ in the solution. In addition to
16 mesh-1B, we tested CO_2 gas permeability of other materials (mesh-2B, PTFE-1B and -2B,
17 fabrics-1B and -2B, and paper-B) coated with the PDMS-coated SiO_2 nanoparticles via dip-
18 coating in solution B. In all vials wrapped with these superhydrophobic films, CaCO_3
19 precipitations were observed, which indicates that the films offered permeability for CO_2 gas.

20 Using the experimental set-up with SPME shown in Fig. 2c, the gas permeability of the
21 solution-B-treated meshes, PTFE membranes, paper, and fabrics were quantitatively analyzed in
22 greater depth. As shown in Table 2, the amount of DMMP vapor captured by the SPME fiber
23 with meshes-B between DMMP liquid and SPME fiber reached over 90% of the respective value

1 of the situation without the superhydrophobic shield. PTFE films-B reached over 70% of
2 permeability and gas permeability of paper-B, fabric-1B and 2B were 53%, 29% and 69%,
3 respectively. For comparison, gas permeability of a commercial umbrella fabric was tested and
4 determined to be 40%. It is worth noting that DMMP is a chemical warfare agent, making
5 detection of its vapor very important.³² After the gas permeability test, the water contact angle
6 did not change significantly, and the superhydrophobic properties of the surfaces were
7 maintained.

8 Table 3 shows waterproof ability of the fabricated films and commercial umbrella fabric.
9 PTFE-1B withstood the water level more than 4000 mm H₂O, which was beyond the limit of our
10 experimental condition. The PTFE-2B and fabric 2 also had higher waterproof ability compared
11 to that of umbrella fabric, suggesting that those can completely block the penetration of water
12 even under heavy rain. In case of meshes-B, water penetrated through mesh surface as soon as
13 the water was poured from the 4 m height, even though the water droplet falling from a lower
14 height did not penetrate through the mesh. The meshes-B could be the best materials for the
15 selective permeation of gas, when only gas permeability is considered, however, when the sensor
16 should be used under circumstance of certain water pressures, shielding layers based on PTFE
17 can be a better choice due to its higher waterproof ability and relatively high gas permeability.

18 It is challenging to concrete the relationship between substrate structure and gas permeability
19 or waterproof ability. Nonetheless, it seems that both the pore structure and thickness of the
20 substrate can have effect on gas permeability and waterproof ability. Mesh-1B, for example, has
21 micrometer scale pore size and therefore it can easily reach the gas permeability ratio of 100%.
22 On the other hand, although the pore size of the PTFE-1B is much smaller than that of mesh-1,
23 the gas permeable ratio of PTFE-1B was over 70% since the film is very thin (~ 30 μm). The

1 waterproof ability can be related to not only pore size but also pore structure of the substrates.
2 Mesh-1B has aligned micrometer scale pores with high regularity, and therefore it is hard for
3 mesh-1B to bare the water pressure and block the water penetration. On the other hand, PTFE-
4 1B is composed of stacks of poorly aligned nanometer scale pores connected by irregular
5 channels, which can help the substrates endure the pressure of water column. Since
6 superhydrophobic coating does not have much influence on the internal pore structures of films,
7 we suggest that the gas permeability is not much influenced by the superhydrophobic coating.

8

9 **Conclusions**

10 In this work, we reported a simple and versatile method for the fabrication of
11 superhydrophobic films with gas permeability using a dip-coating process. The high water
12 repellent property of coated substrates was revealed by measuring the water contact angle on the
13 film surface. Also, by adding PDMS and curing agent to the coating solution, adhesion of
14 PDMS-coated silica nanoparticles to a substrate was enhanced. Even after being exposed to
15 acidic and basic environments and UV-irradiation, the superhydrophobicity of the films was
16 maintained. We also demonstrated the fabrication of a gas permeable membrane with highly
17 water repellent properties using our method. The superhydrophobic and gas permeable
18 membrane can be used as a shielding layer in gas sensors, thus preventing contamination of the
19 sensor with aqueous liquids.

20

21 **Acknowledgment**

22 This research was supported by the Civil-Military Technology Cooperation Program.

23

1 **References**

- 2 1. W. Barthlott, T. Schimmel, S. Wiersch, K. Koch, M. Brede, M. Barczewski, S. Walheim,
3 A. Weis, A. Kaltenmaier, A. Leder and H. F. Bohn, *Adv.Mater.*, 2010, **22**, 2325.
- 4 2. L. Feng, S. Li, Y. Li, H. Li, L. Zhang, J. Zhai, Y. Song, B. Liu, L. Jiang and D. Zhu, *Adv.*
5 *Mater.*, 2002, **14**, 1857.
- 6 3. M. Qu, B. Zhang, S. Song, L. Chen, J. Zhang and X. Cao, *Adv. Funct. Mater.*, 2007, **17**,
7 593.
- 8 4. A. Tuteja, W. Choi, M. Ma, J. M. Mabry, S. A. Mazzella, G. C. Rutledge, G. H.
9 McKinley and R. E. Cohen, *Science*, 2007, **318**, 1618.
- 10 5. Y. Lee, S. H. Park, K. B. Kim and J. K. Lee, *Adv. Mater.*, 2007, **19**, 2330.
- 11 6. T. Sun, L. Feng, X. Gao and L. Jiang, *Accounts Chem. Res.*, 2005, **38**, 644.
- 12 7. G. Caputo, B. Cortese, C. Nobile, M. Salerno, R. Cingolani, G. Gigli, P. D. Cozzoli and
13 A. Athanassiou, *Adv. Funct. Mater.*, 2009, **19**, 1149.
- 14 8. R. A. Gittens, T. McLachlan, R. Olivares-Navarrete, Y. Cai, S. Berner, R. Tannenbaum,
15 Z. Schwartz, K. H. Sandhage and B. D. Boyan, *Biomaterials*, 2011, **32**, 3395.
- 16 9. J. Park, H. Lim, W. Kim and J. S. Ko, *J.Colloid. Interf. Sci.*, 2011, **360**, 272.
- 17 10. B. Deng, R. Cai, Y. Yu, H. Q. Jiang, C. L. Wang, J. A. Li, L. F. Li, M. Yu, J. Y. Li, L. D.
18 Xie, Q. Huang and C. H. Fan, *Adv. Mater.*, 2010, **22**, 5473.
- 19 11. S. Ramakrishna, K. S. S. Kumar, D. Mathew and C. P. R. Nair, *J. Mater. Chem. A*, 2015,
20 **3**, 1465.
- 21 12. X. Deng, L. Mammen, H. J. Butt and D. Vollmer, *Science*, 2012, **335**, 67.
- 22 13. Y. C. Jung and B. Bhushan, *ACS Nano*, 2009, **3**, 4155.

- 1 14. T. Verho, C. Bower, P. Andrew, S. Franssila, O. Ikkala and R. H. A. Ras, *Adv. Mater.*,
2 2011, **23**, 673.
- 3 15. D. Wang, Z. B. Zhang, Y. M. Li and C. H. Xu, *Acs Appl. Mater. Interfaces*, 2014, **6**,
4 10014.
- 5 16. H. X. Wang, Y. H. Xue, J. Ding, L. F. Feng, X. G. Wang and T. Lin, *Angew. Chem. Int.*
6 *Edit.*, 2011, **50**, 11433.
- 7 17. C. R. Crick, J. A. Gibbins and I. P. Parkin, *J. Mater. Chem. A*, 2013, **1**, 5943.
- 8 18. C. X. Wang, T. J. Yao, J. Wu, C. Ma, Z. X. Fan, Z. Y. Wang, Y. R. Cheng, Q. Lin and B.
9 Yang, *Acs Appl. Mater. Interfaces*, 2009, **1**, 2613.
- 10 19. F. J. Wang, S. Lei, C. Q. Li, J. F. Ou, M. S. Xue and W. Li, *Ind. Eng. Chem. Res.*, 2014,
11 **53**, 7141.
- 12 20. W. Barthlott and C. Neinhuis, *Planta*, 1997, **202**, 1.
- 13 21. B. Bhushan, Y. C. Jung and K. Koch, *Philos. T. R. SOC. A.*, 2009, **367**, 1631.
- 14 22. B. Bhushan, K. Koch and Y. C. Jung, *Ultramicroscopy*, 2009, **109**, 1029.
- 15 23. I. Sas, R. E. Gorga, J. A. Joines and K. A. Thoney, *J. Polym. Sci. Pol. Phys.*, 2012, **50**,
16 824.
- 17 24. J.-G. Kim, H. J. Choi, K.-C. Park, R. E. Cohen, G. H. McKinley and G. Barbastathis,
18 *Small*, 2014, **10**, 2487.
- 19 25. M. Sakhuja, J. Son, H. Yang, C. S. Bhatia and A. J. Danner, *Sol. Energy*, 2014, **110**, 231.
- 20 26. J. Son, S. Kundu, L. K. Verma, M. Sakhuja, A. J. Danner, C. S. Bhatia and H. Yang, *Sol.*
21 *Energ. Mat. Sol. C.*, 2012, **98**, 46.
- 22 27. R. N. Gillanders, M. C. Tedford, P. J. Crilly and R. T. Bailey, *Anal. Chim. Acta.*, 2005,
23 **545**, 189.

- 1 28. C. K. Ho and R. C. Hughes, *Sensors*, 2002, **2**, 23.
- 2 29. O. Knopfmacher, M. L. Hammock, A. L. Appleton, G. Schwartz, J. Mei, T. Lei, J. Pei
3 and Z. Bao, *Nat. Commun.*, 2014, **5**, 2954.
- 4 30. Y. K. Cho, E. J. Park and Y. D. Kim, *J. Ind. Eng. Chem.*, 2014, **20**, 1231.
- 5 31. Y. H. Kim, M. G. Jeong, H. O. Seo, S. Y. Park, I. B. Jeong, K. D. Kim, S. M. Cho, D. C.
6 Lim and Y. D. Kim, *Appl. Surf. Sci.*, 2012, **258**, 7562.
- 7 32. E. J. Park, Y. K. Cho, D. H. Kim, M. G. Jeong, Y. H. Kim and Y. D. Kim, *Langmuir*,
8 2014, **30**, 10256.
- 9 33. E. J. Park, K. D. Kim, H. S. Yoon, M. G. Jeong, D. H. Kim, D. C. Lim, Y. H. Kim and Y.
10 D. Kim, *RSC Adv.*, 2014, **4**, 30368.
- 11 34. E. J. Park, J. K. Sim, M. G. Jeong, H. O. Seo and Y. D. Kim, *RSC Adv.*, 2013, **3**, 12571.
- 12 35. H. O. Seo, M.-G. Jung, K.-D. Kim, Y. D. Kim, D. Chan Lim and K. H. Lee, *Curr. Appl.*
13 *Phys.*, 2013, **13**, 31.
- 14 36. V. Barbier, M. Tatoulian, H. Li, F. Arefi-Khonsari, A. Ajdari and P. Tabeling, *Langmuir*,
15 2006, **22**, 5230.
- 16 37. M. D. Alba, Z. Luan and J. Klinowski, *J. Phys. Chem.*, 1996, **100**, 2178.
- 17 38. J. Shen, A. Luo, L. Yao, X. Lin, B. Zhou, G. Wu and X. Ni, *Mat. Sci. Eng. C-Bio. S.*,
18 2007, **27**, 1145.
- 19 39. J. Coates, in *Encyclopedia of Analytical Chemistry*, ed. R.A. Meyers, Newtown, 2000, Ch.
20 2, pp. 2-4.
- 21 40. A. Mata, A. Fleischman and S. Roy, *Biomed Microdevices*, 2005, **7**, 281.
- 22 41. G. Orcel, J. Phalippou and L. L. Hench, *J. Non-Cryst. Solids.*, 1986, **88**, 114.
- 23

1 **Caption**

2 **Fig. 1** Schematic diagram of the experimental set-up for (a) the preparation of hydrophobic
3 coating on silica nanoparticles, and (b) the preparation of dip-coating solution and
4 superhydrophobic films.

5 **Fig. 2** Schematic description of the experimental set-up for (a) sand abrasion experiment, (b) gas
6 permeation test, and (c) gas permeability measurement using SPME.

7 **Fig. 3** (a) FT-IR spectra of silica nanoparticles before and after PDMS-coating. (b) Images after
8 dispersing bare (left) and PDMS-coated (right) silica nanoparticles in distilled water.

9 **Fig. 4** SEM images of (a) plain metal mesh-1, (b) magnified image of (a), (c) dip-coated metal
10 mesh-1B, and (d) magnified image of (c). EDS mapping images of (e) Si and (f) C for the SEM
11 image of (c).

12 **Fig. 5** Change in water contact angle of mesh-1A and -1B as a function of amount of sand
13 dropped onto the surface.

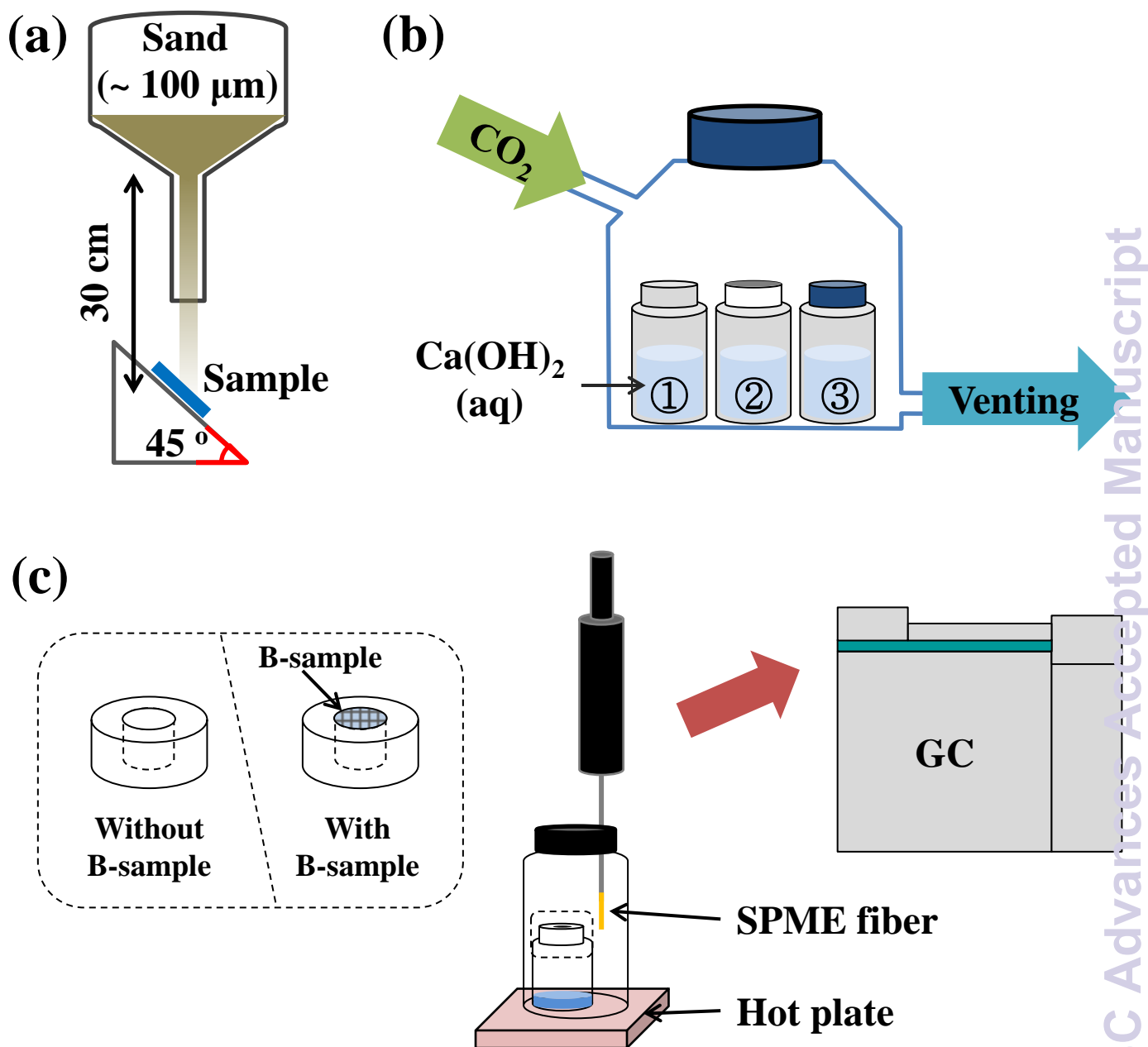
14 **Fig. 6** SEM images after the sand abrasion test on (a) mesh-1A, (b) magnification of (a); and (c)
15 mesh-1B, (d) magnification of (c).

16 **Fig. 7** Change in water contact angle as a function of mesh-1B surface exposure to (a) acidic
17 (HCl (aq), pH 2.5) and basic (NaOH (aq), pH 12) conditions and (b) UV irradiation.

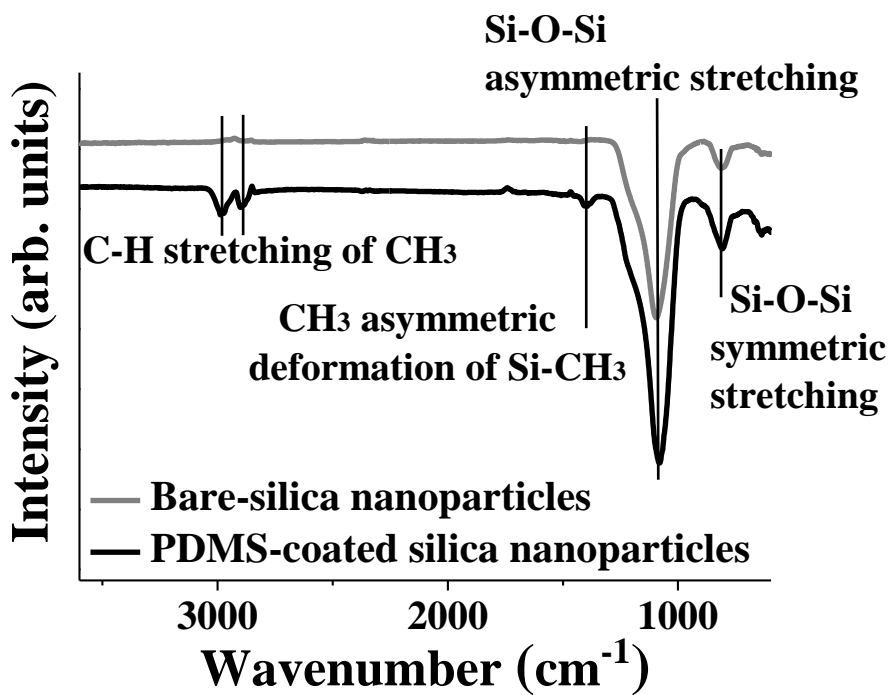
18 **Fig. 8** Images of vials containing $\text{Ca}(\text{OH})_2$ solution before (left) and after (right) the gas
19 permeation test. ① Without cap (open), ② With a dip-coated mesh-1B, ③ With cap (sealed).

- 1 **Table 1** The static water contact angles (θ_{sta}) of various substrates before and after dip-coating,
- 2 and water contact angle hysteresis ($\theta_{ad} - \theta_{re}$) values of substrates after dip-coating.
- 3 **Table 2** Gas permeability measurements on various substrates.
- 4 **Table 3** Waterproof ability evaluation on various substrates.

Fig. 2

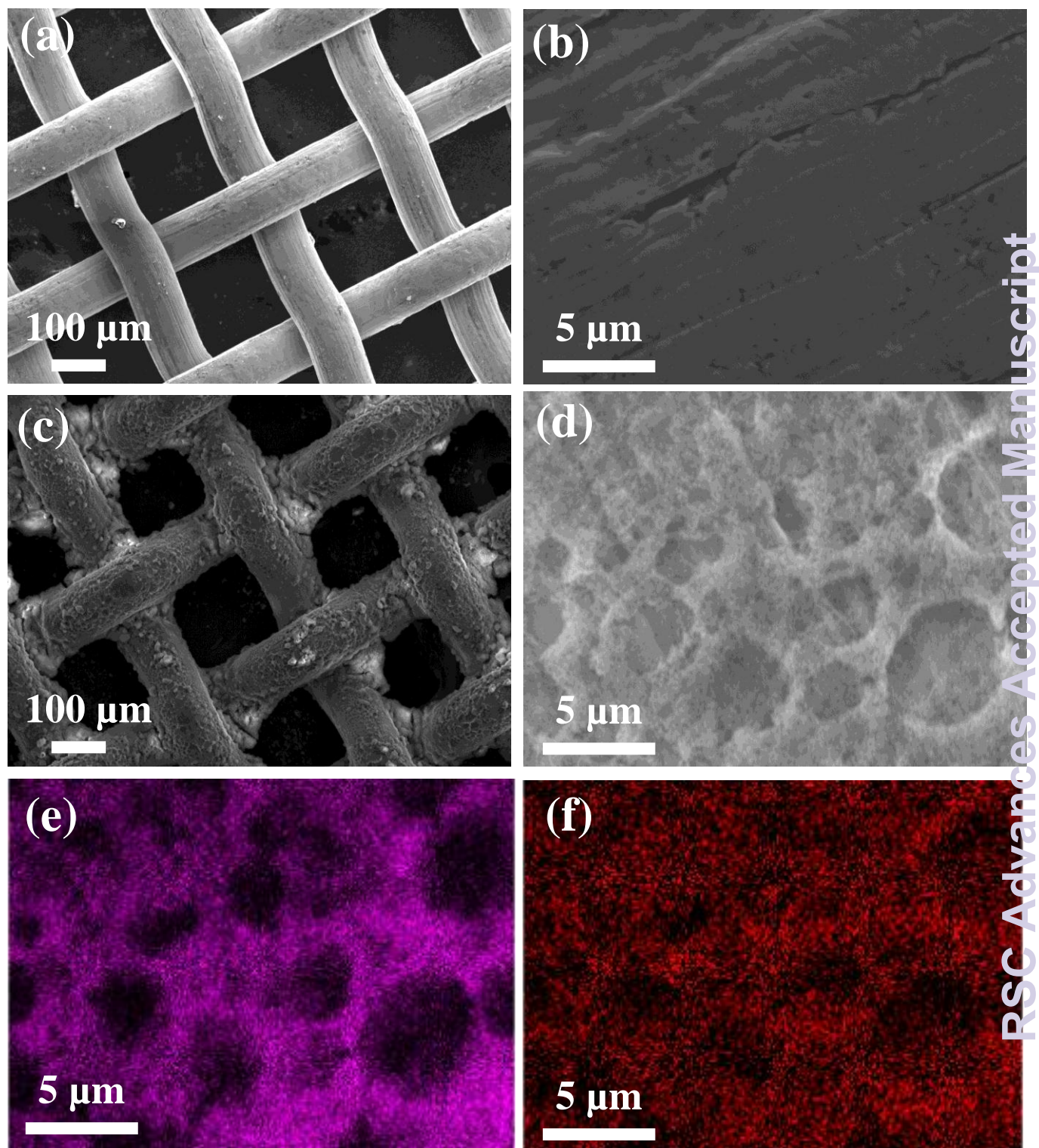


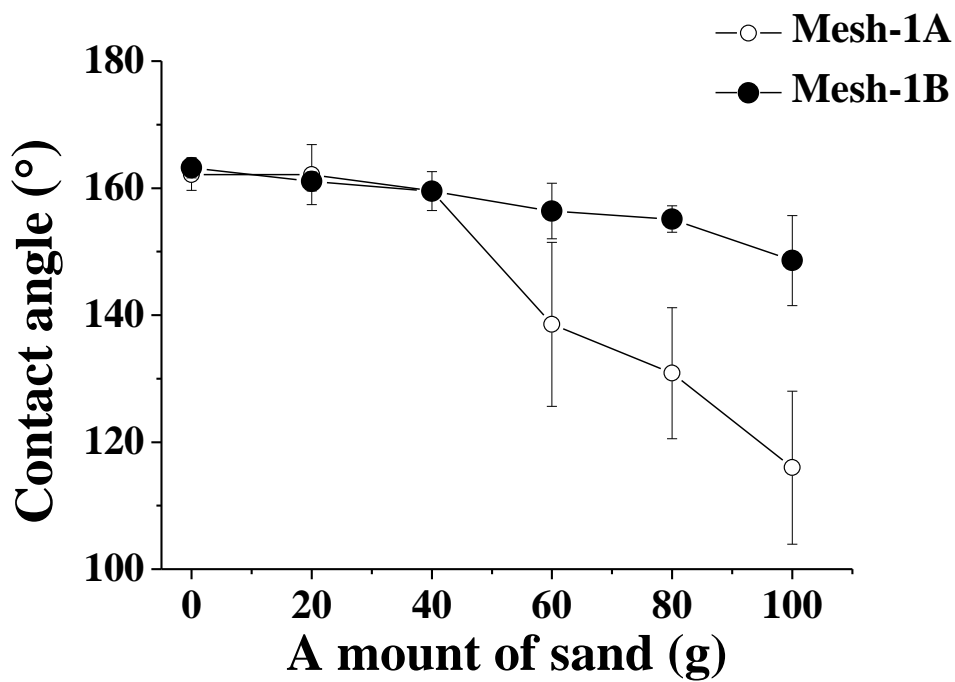
(a)

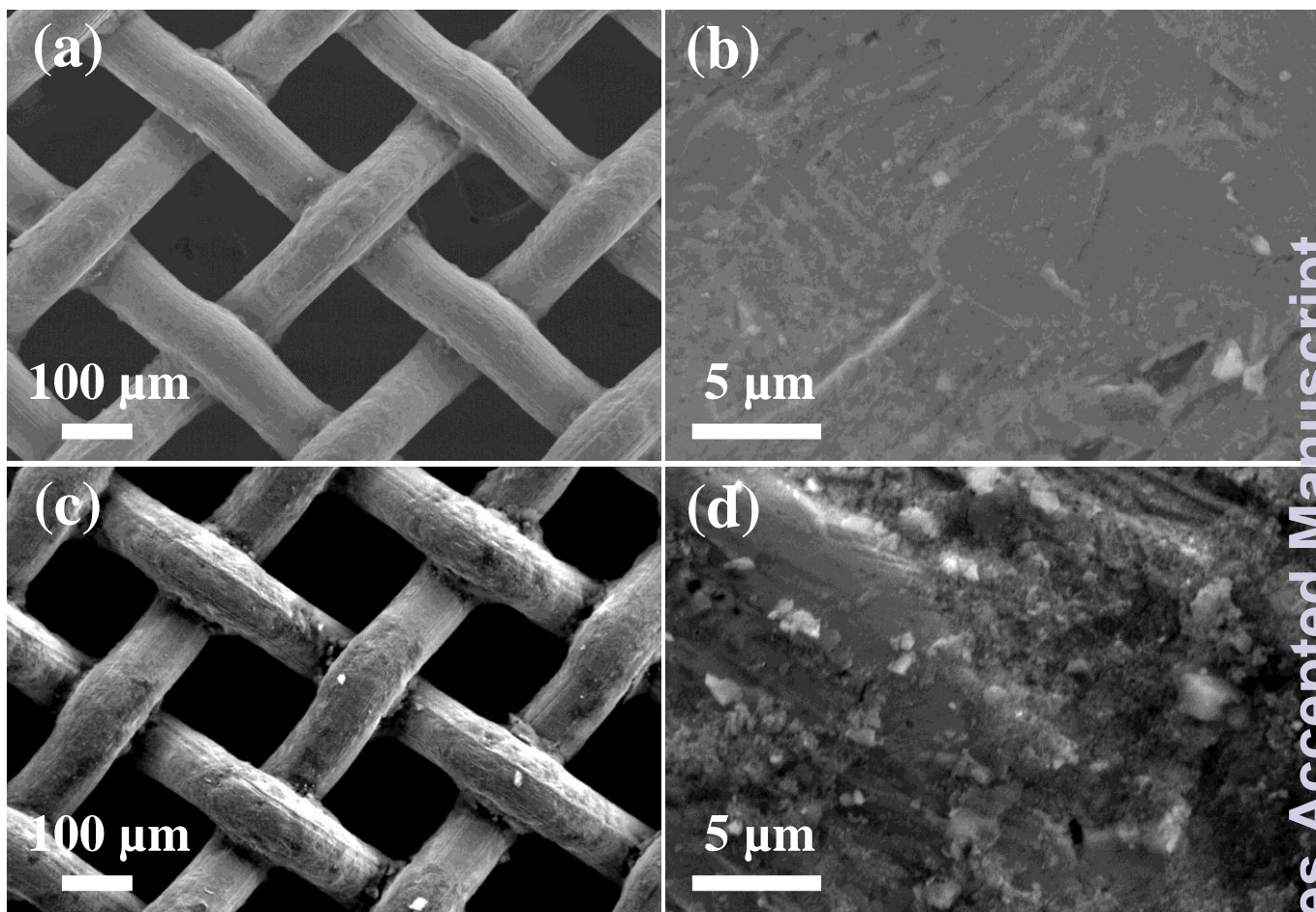


(b)

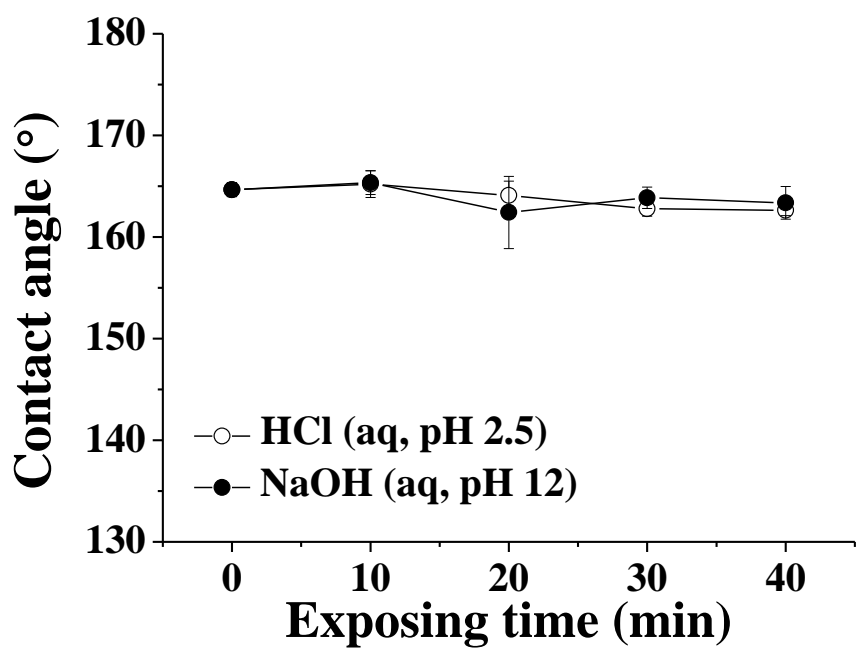


Fig. 4

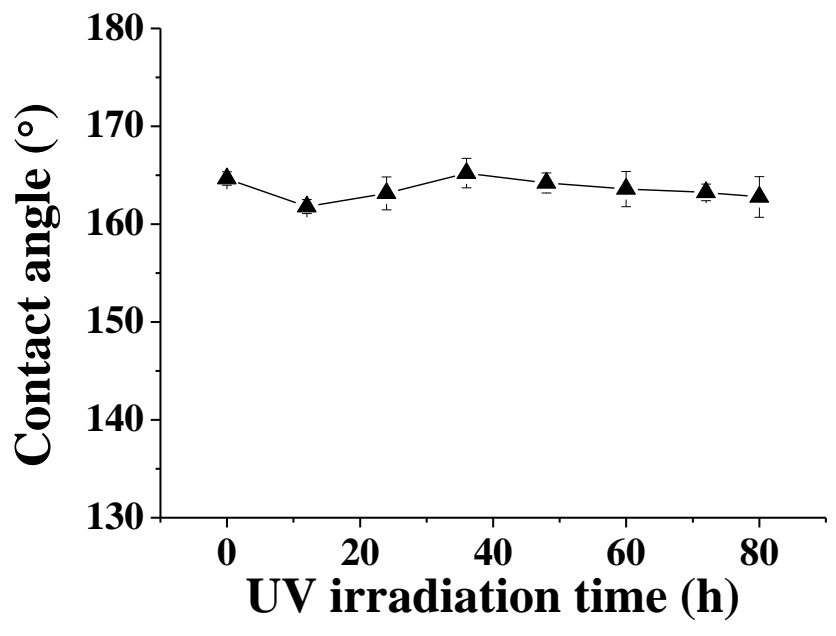




(a)



(b)



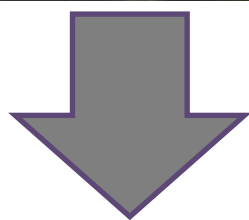


Table 1

Sample	Bare (°)	Coated film (°)			
	θ_{sta}	θ_{sta}	θ_{ad}	θ_{re}	$\theta_{ad} - \theta_{re}$
Mesh-1B	117.6	166.0	162.5	159.1	3.4
Mesh-2B	113.3	160.4	161.5	154	7.5
PTFE-1B	137.3	163.2	162.8	155.1	7.7
PTFE-2B	138.7	162.3	159.4	154.8	4.6
Paper-B	139.2	162.6	158.9	156.1	2.8
Fabric-1B	111.1	163.8	161.2	154.6	5.6
Fabric-2B	44	161.0	160.7	155	5.7

Sample	Gas permeability
Mesh-1B	100%
Mesh-2B	91%
PTFE-1B	71%
PTFE-2B	77%
Paper-B	53%
Fabric-1B	29%
Fabric-2B	69%
Umbrella	40%

Table 3

Sample	Waterproof (mmH₂O)
Mesh-1B	-
Mesh-2B	-
PTFE-1B	> 4000
PTFE-2B	3300
Paper-B	190
Fabric-1B	180
Fabric-2B	733
Umbrella	402